


Centrifugal effects on the dynamic characteristics of high speed hydrostatic thrust bearing lubricated by low viscosity fluid

Proc IMechE Part J:
J Engineering Tribology
0(0) 1–12
© IMechE 2014
Reprints and permissions:
sagepub.co.uk/journalsPermissions.nav
DOI: 10.1177/1350650114534403
pij.sagepub.com


Lei Wang and Shuyun Jiang

Abstract

The effect of the centrifugal force of the fluid film on the performance of the high speed hydrostatic thrust bearing lubricated by low viscosity fluid cannot be neglected. Considering the centrifugal inertia effect, concentrated inertia effect at the recess edge, and the misalignment effect, the thermo-hydrodynamic lubrication model is established by using the reduced Navier–Stokes equation, the energy equation, and the bulk flow theory. The effects of centrifugal forces on dynamic performances of the high speed thrust bearing with different supply pressures and rotational speeds have been analyzed systematically. The results show that the centrifugal force reduces the axial and angular stiffness and hardly affects the damping coefficients; the centrifugal effects decrease with the increasing of eccentricity ratio and misalignment angle.

Keywords

Centrifugal force, thrust bearing, low viscosity fluid, dynamic characteristics, turbulent

Date received: 9 October 2013; accepted: 24 March 2014

Introduction

Fluid bearing lubricated by low viscosity lubricant, such as water, refrigerant, and so forth, has been used in high speed rotating machinery.^{1,2} With the increasing of the rotating speed, the centrifugal effect of the fluid film on the bearing performance cannot be neglected, for example, the centrifugal force can lead to sub-ambient pressure and may induce lubricant cavitations for the fluid bearing. Several previous studies have shown that centrifugal force has a remarkable effect on the characteristics of high speed thrust bearing, and Navier–Stokes equation was simplified to obtain the momentum equation with centrifugal force in laminar or turbulent flow regime. The load capacity, flow rate, and power loss in high speed thrust bearing including centrifugal effects have been thoroughly discussed.^{3–14} The following review details some important investigation carried out for the thrust bearing with centrifugal effects.

Dowson and Coombs^{3,4} first introduced the theoretical and experimental analysis of the centrifugal effects on hydrostatic thrust bearing performance for isothermal lubricants. The momentum equation was simplified in one dimension, and the thermal effect was neglected in the theoretical analysis. Furthermore, thermal effect was considered in the analysis of the centrifugal effects on performance of

hydrodynamic thrust bearings by Pinkus and Lund⁵ and Dareing and Chen.⁶ In the thermo-hydrodynamic lubrication analysis, Pinkus and Lund⁵ and Dareing and Chen⁶ established two-dimensional momentum equations with the laminar flow regime considered. And then some researchers proposed the theoretical models considering coupled centrifugal inertia and turbulent effect,^{7,10} as well as coupled centrifugal and misalignment effect^{11,12} to analyze the performance of hydrodynamic and hydrostatic thrust bearing. Other studies have focused on the effects of centrifugal forces on the performance of the thrust bearing with surface roughness effect¹³ or the two-phase flow.¹⁴

The above studies have been instrumental in building a better understanding of this area of research. However, most of these studies only investigated the centrifugal effects on steady state performance of thrust bearings and to the best of the authors' knowledge, no attempt has been made yet to study the

School of Mechanical Engineering, Southeast University, PR China

Corresponding author:

Shuyun Jiang, School of Mechanical Engineering, Southeast University, Southeast Road 2#, Jiangning District, Nanjing 211189, PR China.
Email: jiangshy@seu.edu.cn

centrifugal effects on the dynamic performance of thrust bearing considering the turbulent flow regime and misalignment condition in thermo-hydrodynamic lubrication analysis.

In this study, an analysis is conducted and solutions are provided for the effect of centrifugal forces on dynamic performance of high speed hydrostatic thrust bearing lubricated by water. Considering the centrifugal inertia effect, concentrated inertia effect at the recess edge, and the misalignment effect, the thermo-hydrodynamic lubrication model is established by using the reduced Navier–Stokes equation, the energy equation, and the bulk flow theory. The effects of centrifugal forces on the dynamic performances of the high speed hydrostatic water-lubricated thrust bearing have been analyzed systematically under different supply pressures and rotational speeds.

Theoretical analysis

Geometry of hydrostatic thrust bearing

Figure 1 shows the geometry of the hydrostatic thrust bearing with four recesses and feed orifices.

Turbulent Reynolds equation

1. The Navier–Stokes equations with centrifugal forces for thrust bearing are given by¹⁵

$$\frac{\partial \tau_{\theta z}}{\partial z} = \frac{1}{r} \left(\frac{\partial p}{\partial \theta} \right) \quad (1)$$

$$\frac{\partial \tau_{Rz}}{\partial z} = \frac{\partial p}{\partial r} - \frac{\rho u_{\theta}^2}{r} \quad (2)$$

$$\frac{\partial}{\partial r}(r u_r) + \frac{\partial}{\partial \theta}(u_{\theta}) + r \frac{\partial}{\partial z}(u_z) = 0 \quad (3)$$

where u_{θ} , u_r , and u_z are circumferential, radial, and axial velocities and $\tau_{\theta z}$ and τ_{Rz} are wall shear stresses.

Bulk-flow velocities are defined as the mean values across the film thickness, i.e.

$$V_{\theta} = \frac{1}{h} \int_0^h u_{\theta} dz, \quad V_r = \frac{1}{h} \int_0^h u_r dz \quad (4)$$

where V_{θ} , V_r are circumferential and radial velocities of the bulk flow.

Integration of the governing equations (1) to (3) across the film thickness (axial direction) leads to

$$\tau_{\theta z}|_0^h = \frac{h}{r} \left(\frac{\partial p}{\partial \theta} \right) \quad (5)$$

$$\tau_{Rz}|_0^h = h \frac{\partial p}{\partial r} - \frac{\rho I_{\theta}}{r} \quad (6)$$

$$\frac{\partial}{\partial \theta}(h V_{\theta}) + \frac{\partial}{\partial r}(r \cdot h \cdot V_r) + r \cdot \frac{\partial h}{\partial t} = 0 \quad (7)$$

The moment-flux integrals in equation (6) are

$$I_{\theta} = \int_0^h u_{\theta}^2 dz \quad (8)$$

2. The inertia terms I_{θ} are calculated in the manner suggested by Constantinescu and Galetuse,¹⁶ i.e.

$$I_{\theta} = \int_0^h u_{\theta}^2 dz = \alpha V_{\theta}^2 \cdot h + \delta U^2 \cdot h - r V_{\theta} U h \quad (9)$$

In the turbulent flow,

$$\alpha \cong 1, \quad \delta \cong \frac{0.885}{\text{Re}^{0.367}}, \quad r \cong 0, \quad \text{Re} = \frac{\rho \omega r h}{\mu}$$

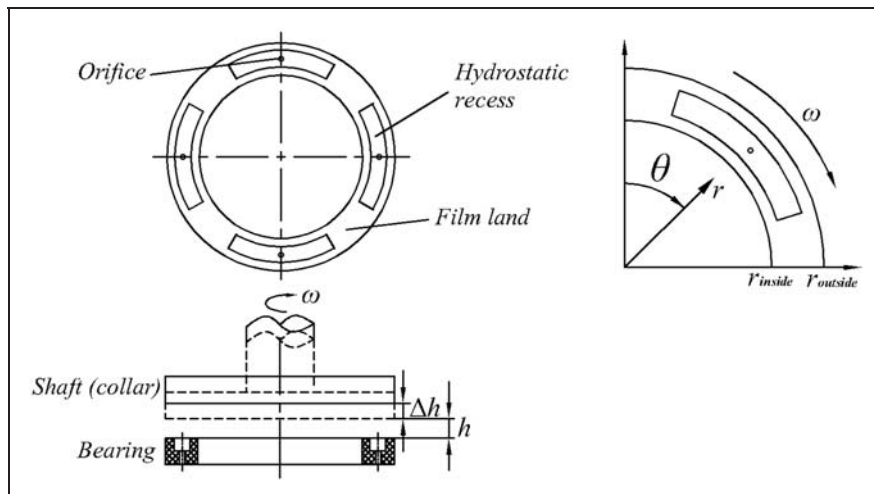


Figure 1. Geometry of the hydrostatic thrust bearing.

Then

$$I_\theta = \int_0^h u_\theta^2 dz = V_\theta^2 \cdot h + \delta(\omega r)^2 \cdot h \quad (10)$$

3. Based on the bulk-flow theory,^{10,17,18} the wall shear stress in terms of the bulk flow velocity components are as follows

$$\tau_{\theta z}|_0^h = -\frac{\mu}{h} \left(k_\theta V_\theta - \frac{1}{2} k_J \cdot \omega \cdot r \right) \quad (11)$$

$$\tau_{rz}|_0^h = -\frac{\mu}{h} k_r V_r \quad (12)$$

where the turbulent flow shear factors (k_θ , k_r) that depend on turbulent shear parameters at shaft and bearing are given by^{10,17,18}

$$k_\theta = k_r = \frac{1}{2} (k_J + k_B) \quad (13)$$

where the turbulent shear parameters at shaft and bearing (k_J , k_B) are defined in terms of the flow Reynolds numbers relative to the rotating shaft and stationary bearing surfaces^{10,17,18}

$$k_J = 0.066 \text{Re}_J^{0.75}, \quad k_B = 0.066 \text{Re}_B^{0.75} \quad (14)$$

The flow Reynolds numbers relative to the rotating shaft and stationary bearing surfaces are^{10,17,18}

$$\text{Re}_J = \frac{\rho h}{\mu} [(V_\theta - \omega r)^2 + V_r^2]^{\frac{1}{2}}, \quad \text{Re}_B = \frac{\rho h}{\mu} [V_\theta^2 + V_r^2]^{\frac{1}{2}} \quad (15)$$

4. Substituting equations (11) and (12) into equations (5) and (6), the averaged momentum equations are obtained as

$$\frac{h}{r} \left(\frac{\partial p}{\partial \theta} \right) = -\frac{\mu}{h} \left(k_\theta V_\theta - \frac{1}{2} k_J \cdot \omega \cdot r \right) \quad (16)$$

$$h \frac{\partial p}{\partial r} - \frac{\rho V_\theta^2 \cdot h}{r} - \frac{\rho \delta (\omega r)^2 \cdot h}{r} = -\frac{\mu}{h} k_r V_r \quad (17)$$

From the above equation, the Bulk-flow velocities V_θ and V_r are obtained as

$$V_\theta = -\frac{\frac{2h^2}{\mu r} \left(\frac{\partial p}{\partial \theta} \right) - k_J \cdot \omega \cdot r}{(k_B + k_J)} \quad (18)$$

$$V_r = -\frac{\frac{2h^2}{\mu} \frac{\partial p}{\partial r} - \frac{2\rho V_\theta^2 \cdot h^2}{\mu r} - \frac{2\rho \delta (\omega r)^2 \cdot h^2}{\mu r}}{(k_B + k_J)} \quad (19)$$

When equations (18) and (19) are inserted into the continuity equation (7) and the terms grouped together, we obtain

$$\begin{aligned} & \frac{1}{r} \frac{\partial}{\partial \theta} \left(\frac{h^3}{\mu(k_B + k_J)} \frac{\partial p}{\partial \theta} \right) + \frac{\partial}{\partial r} \left(\frac{r \cdot h^3}{\mu(k_B + k_J)} \frac{\partial p}{\partial r} \right) \\ &= \frac{\omega \cdot r}{2} \frac{\partial}{\partial \theta} \left(\frac{k_J}{(k_B + k_J)} h \right) + \rho \omega^2 \frac{\partial}{\partial r} \left(\frac{k_J^2}{\mu(k_B + k_J)^3} r^2 \cdot h^3 \right) \\ &+ \rho \omega^2 \frac{\partial}{\partial r} \left(\frac{\delta r^2 h^3}{\mu(k_B + k_J)} \right) + \frac{r}{2} \cdot \frac{\partial h}{\partial t} \\ &\times \rho \frac{\partial}{\partial r} \left(\frac{4h^5 \left(\frac{\partial p}{\partial \theta} \right) \left(\left(\frac{h^2}{\mu r^2} \frac{\partial p}{\partial \theta} \right) - k_J \cdot \omega \right)}{\mu^2 (k_B + k_J)^3} \right) \end{aligned} \quad (20)$$

The above is turbulent Reynolds equation, containing the effects of centrifugal forces in the fluid film.

5. The Local acceleration of fluid film from a deep recess into the film lands cause a sudden pressure drop in the high speed condition, the pressure at the entrance to the film lands is modeled from Bernoulli's equation as¹⁸

$$p_e = p_r - \frac{\rho V_{\theta,r}^2}{2} (1 + \xi) \quad (V_{\theta,r} \cdot n > 0) \quad (21)$$

where P_r is recess pressure and ξ is empirical entrance loss coefficient.

Note that the entrance loss coefficient ξ is expressed as the empirical (edge) entrance loss coefficients and the entrance loss coefficients in the study by Arghir et al.¹⁹ are used in this study due to good agreement with the experimental results.

Energy equation

The energy equation for adiabatic conditions under turbulent flow regime is obtained as follows^{20,21}

$$\rho \left[\frac{\partial (c_v T h V_\theta)}{r \partial \theta} + \frac{\partial (c_v T h V_r)}{\partial r} \right] = \tau_{\theta z}|_0 \omega \cdot r - \tau_{\theta z}|_0^h V_\theta - \tau_{rz}|_0^h V_r \quad (22)$$

where C_v represents the heat capacity of lubricant

$$\tau_{\theta z}|_0 = \frac{1}{2} h \frac{\partial p}{\partial \theta} + \frac{\mu}{4h} [k_b V_\theta - k_J (V_\theta - \omega \cdot r)] \quad (23)$$

$$\tau_{\theta z}|_0^h = -\frac{\mu}{h} \left(k_\theta V_\theta - k_J \frac{\omega \cdot r}{2} \right) \quad (24)$$

$$\tau_{rz}|_0^h = -\frac{\mu}{h} (k_r V_r) \quad (25)$$

The water viscosity is considered to vary with temperature according to the following formula²²

$$\mu = \frac{0.001779}{1 + 0.03368T + 0.000221T^2} \quad (26)$$

Mass conservation at a recess

The continuity equation at the recess is defined by the global balance between the flow through the orifice restrictor (Q_{in}), the recess outflow into the film lands (Q_{out}), and the time rate of mass changing due to squeeze effect (Q_j). The recess flow continuity equation is expressed as

$$Q_{in} = Q_{out} + Q_j \quad (27)$$

where the flow through the orifice restrictor is

$$Q_{in} = A_0 C_d \sqrt{2(p_s - p_r)/\rho} \quad (28)$$

where C_d is the discharge coefficient of the orifice restrictor related to the pressure drop law of the orifice, and C_d of 0.8 is chosen according to the recommended value in the literature.²³

The recess outflow into the film lands comprises two parts, the flow across axial and circumferential boundaries of the recess

$$Q_{out} = Q_{outa} + Q_{outc} \quad (29)$$

The time rate of mass changing due to squeeze effect is determined as follows

$$Q_j = A_r \frac{\partial h}{\partial t} \quad (30)$$

Global energy balance equation at a recess

As is shown in Figure 2, the energy leaving the boundary of a bearing recess must be equal to the energy flowing into a bearing recess

$$E_{in} = E_{out} \quad (31)$$

1. The energy flowing into a bearing recess comprises two parts, the carry-over of hot fluid from upstream to downstream of the recess and the fresh fluid from the supply source into the recess volume. The energy transport produced by pressure gradient can be neglected due to uniform pressure and high speed circumferential velocity through the recess²⁴

$$E_{in} = Q_{in}T_s + Q_{left}T_{left} \quad (32)$$

2. The energy leaving the boundary of a bearing recess is expressed as

$$E_{out} = Q_{right}T_{right} + Q_{up}T_{up} + Q_{down}T_{down} \quad (33)$$

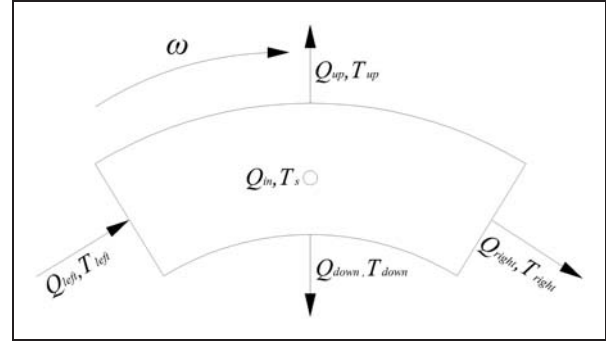


Figure 2. Conceptual description of global energy balance at a recess.

Boundary conditions

The boundary conditions for the hydrostatic thrust bearing from Figure 3 are as given below.

Pressure boundary conditions:

1. The pressure at the inner and outer bearing radius are specified as

$$p(r_{in}) = p_a; \quad p(r_{out}) = p_a$$

2. The pressure in each recess is equal to p_{ri} at the r th recess
3. Fluid inertia at the recess edges is treated through a Bernoulli-type relationship
4. The supply pressure is equal to p_s
5. On the 360° extended film land, the pressure field is continuous and single-valued in the circumferential direction

$$p(r, \theta) = p(r, \theta + 2\pi)$$

Temperature boundary conditions:

1. The temperature in each recess is equal to T_{ri} at the r th recess
2. The temperature of bearing recesses and edges are obtained as described above, i.e.

$$T_{right} = T_{up} = T_{down} = T_{ri}$$

3. The supply temperature is equal to T_s
4. On the 360° extended film land, temperature field is continuous and single-valued in the circumferential direction

$$T(r, \theta) = T(r, \theta + 2\pi)$$

Expression for film thickness

Figure 4 shows the relationship of the film thickness and angular misalignments. h_{xz} and h_{yz} are adopted to

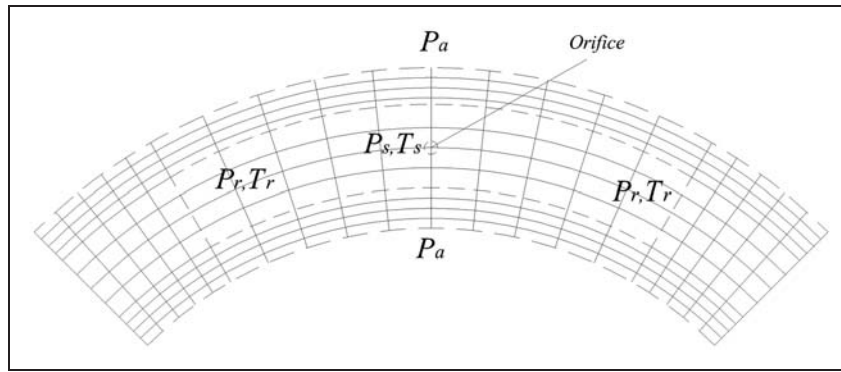


Figure 3. Grid and boundary conditions for finite difference method.

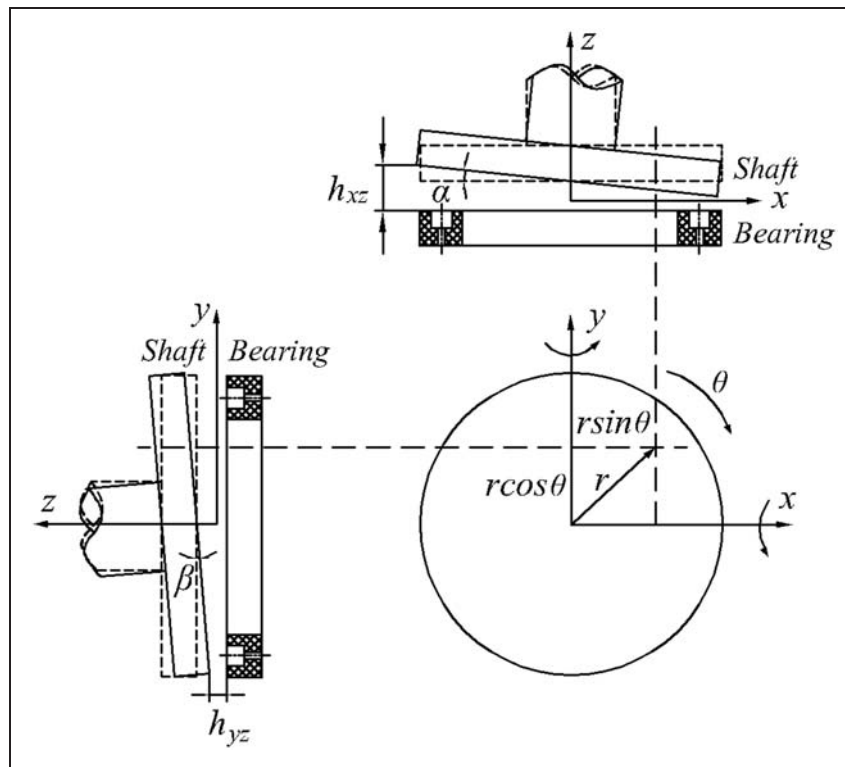


Figure 4. Depiction of shaft collar with angular misalignments.

distinguish different h -s in both views. The film thickness including misalignment of the thrust collar (Figure 4) can be defined by the expression as follows²⁵

$$h = h_0 - t \times h_0 - \alpha \times r \sin \theta + \beta \times r \cos \theta \quad (34)$$

where t is eccentricity ratio of the thrust bearing, $t = \frac{\Delta h}{h_0}$, Δh represents the axial disturbance of the thrust bearing; h_0 is nominal film thickness; and α, β are misalignment angle in XZ -plane and YZ -plane.

Perturbation analysis

The dynamic characteristic of the thrust bearing is modeled as an equivalent spring-damper system;

the perturbation method is used to solve dynamic coefficients.

Consider the thrust collar to undergo small amplitude axial Δz and angular motion $\Delta \alpha$ and $\Delta \beta$ at a frequency ω about an equilibrium position h_0, α_0 , and β_0 . The film thickness and pressure are expressed as the superposition of 0th and first-order fields describing the equilibrium and the perturbed fields,¹² respectively

$$H = h_0(r, \theta) + \Delta z e^{i\omega t} - r \left[\{ \alpha_0 + \Delta \alpha e^{i\omega t} \} \sin \theta - \{ \beta_0 + \Delta \beta e^{i\omega t} \} \cos \theta \right] \quad (35)$$

$$p = p_0(r, \theta, z, \alpha, \beta) + \{ p_z \Delta z + p_\alpha \Delta \alpha + p_\beta \Delta \beta \} e^{i\omega t} \quad (36)$$

where p_z , p_α , and p_β are perturbed pressure along the axial and angle directions.

Integration of the pressure acting on the bearing surface gives the axial force (F_z) and the restoring moments (M_y, M_x), i.e.

$$F_z = \int_{r_0}^{r_3} \int_0^{2\pi} p_0 r dr d\theta \quad (37)$$

$$M_y = \int_{r_0}^{r_3} \int_0^{2\pi} p_0 r \sin \theta r dr d\theta \quad (38)$$

$$M_x = \int_{r_0}^{r_3} \int_0^{2\pi} p_0 r \cos \theta r dr d\theta \quad (39)$$

The represented impedances arise from the dynamic collar motions, i.e.

$$Z_{\phi\phi} = K_{\phi\phi} + i\omega C_{\phi\phi} = - \int_{r_0}^{r_3} \int_0^{2\pi} p_\phi h_\phi r dr d\theta, \quad \phi, \varphi = z, \alpha, \beta \quad (40)$$

where $h_z = 1$; $h_\alpha = \sin \theta$; $h_\beta = \cos \theta$; k_{zz}, c_{zz} are axial dynamic coefficients; and $k_{\alpha\alpha}, k_{\alpha\beta}, k_{\beta\alpha}, k_{\beta\beta}, c_{\alpha\alpha}, c_{\alpha\beta}, c_{\beta\alpha}, c_{\beta\beta}$ are angular dynamic coefficients.

Results and discussion

Based on the above theory, a finite-difference scheme with variable mesh size is implemented to solve the nonlinear differential equations, and the mesh size in recess is twice as the film land, as is shown in Figure 3. A computer program has been developed by using MATLAB tool, and the program flow chart is given in Figure 5.

Model verification

The developed model is verified by computing the load-carrying capacity corresponding to different film clearances (12.7–101.6 μm) and the dimensionless flow rate (with respect to $N_{rec} C_d A_0 (0.5 \rho P_s)^{0.5}$) versus the dimensionless load for a six-recess, orifice compensated, hydrostatic thrust bearing lubricated by R134a refrigerant.¹⁰ The geometry of the hydrostatic thrust bearing is shown in Figure 6, and its parameters are list in Table 1. As is shown in Figure 7, the theoretical results of this study are found to be close to those in the study of Luis,¹⁰ especially for the low supply pressure ($P_s = 1.9 \text{ MPa}$). The difference between this analytical solution and that of Luis¹⁰ may be attributed to the fact that the convective inertia force is not considered for the developed theoretical model.

Dynamic characteristics of the bearing

The parameters of the hydrostatic water-lubricated thrust bearing are listed in Table 2.

Fluid film pressure (P) distribution. Figure 8 displays the pressure fields of water-lubricated thrust bearing. The pressure distribution in the alignment condition is shown in Figure 8. Note the sharp pressure drop at the downstream side of a bearing recess due to the combination of concentrated inertia effect at the recess edge and the centrifugal effects. Meanwhile, Figure 8 depicts the pressure distribution in the misalignment condition ($\alpha = \beta = 2 \times 10^{-4} \text{ rad}$). It is observed that the pressure distribution is not uniform at each recess fields, and the peak pressure is generated at the downstream of one recess fields owing to the hydrodynamic effect.

Fluid film temperature (T) distribution. The temperature profile of water-lubricated thrust bearing is shown in Figure 9. It can be seen that the temperature distributions of both the inner and the outer film lands are roughly similar without considering the misalignment condition, in details, the temperature rise is gradual along the radial direction, and the maximum value is at the outer edge of the water-lubricated thrust bearing. This can be attributed to the fact that the centrifugal force increases apparently along the radial direction of the film land. Figure 9 also shows that the temperature rise of the water-lubricated thrust bearing is not uniformly distributed at each recess field under the misalignment condition and the maximum value can reach 40 °C; this can be caused by the combination of hydrodynamic and turbulent effects.

The axial stiffness coefficients. Figure 10 shows the axial stiffness coefficients of water-lubricated thrust bearing versus the eccentricity ratio under several rotational speeds. The results show that the centrifugal forces reduce the axial stiffness coefficients; when the bearing runs at the rotational speed of 40,000 r/min, the reduction of the axial stiffness coefficient is about 15%, and the centrifugal effects decrease with the increasing of the eccentricity ratio. The axial stiffness reaches the maximum value when the eccentricity ratio is 0.3; this can be attributed to the fact that the bearing has the optimum value of recess pressure with the eccentricity ratio of 0.3. When the eccentricity ratio is less than 0.15, the axial stiffness corresponding to the rotational speed of 20,000 r/min is lower than that of 40,000 r/min; however, as the eccentricity ratio exceeds 0.15, the axial stiffness of 20,000 r/min is greater than that of 40,000 r/min, especially for the high supply pressure of 3 MPa. The authors think that this variation is dominated by the hydrostatic effect for the bearing having a small misalignment angle ($\alpha = \beta = 1 \times 10^{-4} \text{ rad}$).

The axial damping coefficients. The axial damping coefficients as a function of the eccentricity ratio are shown in Figure 11. It is observed that the centrifugal forces reduce the axial damping coefficients, and the reduction of the damping coefficient gets larger with

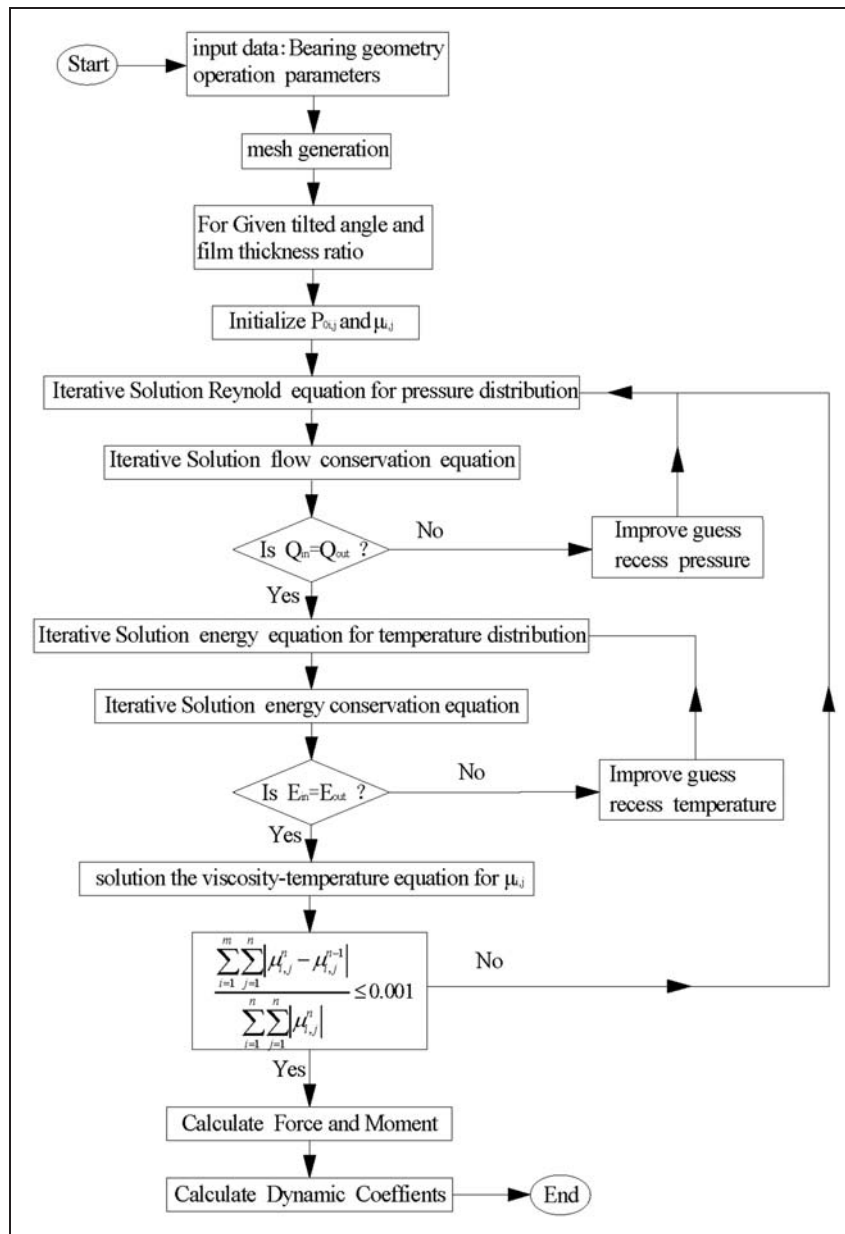


Figure 5. Program flow chart.

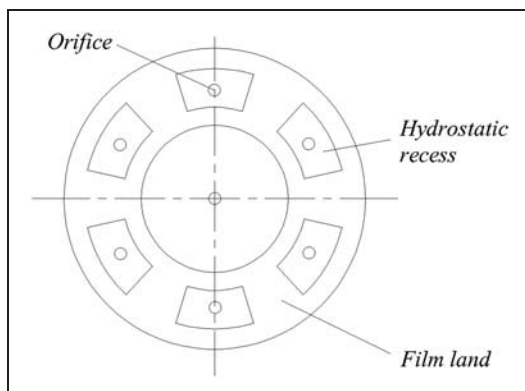


Figure 6. The geometry of hydrostatic thrust bearing.¹⁰

the increase in rotational speed. Moreover, with or without considering the centrifugal effects, the damping coefficients increase gradually with the increase in the eccentricity ratio.

The angular stiffness coefficients. Figure 12 depicts the angular stiffness coefficients of water-lubricated thrust bearing versus the misalignment angle. Note that the centrifugal forces also reduce the angular stiffness coefficients and the centrifugal effects decrease with the increasing of misalignment angle. Meanwhile, the centrifugal forces affect the direct angular stiffness apparently rather than the cross-coupled angular stiffness, especially for the small

Table 1. Parameters of hydrostatic thrust bearing lubricated by R134a refrigerant.¹⁰

Bearing radius (mm)		Nominal film thickness (μm)	
$r_0 = 89.13; r_1 = 102.21; r_2 = 113.89; r_3 = 126.8$		$h_0 = 12 \sim 101$	
Recess depth (mm)	Half angle of recess ($^\circ$)	Orifice diameter (mm)	Supply pressure (MPa)
$h_r = 0.508$	$\theta = 24$	$d_c = 1.7$	$P_s = 1.9, 2.4$
Rotational speed (r/min)	Inlet temperature ($^\circ\text{C}$)	Viscosity (Pa)	Density (kg/m^3)
$\omega = 1 \sim 1.6 \times 10^4$	$T_0 = 38$	$\mu_0 = 0.000198$	$\rho = 1210$

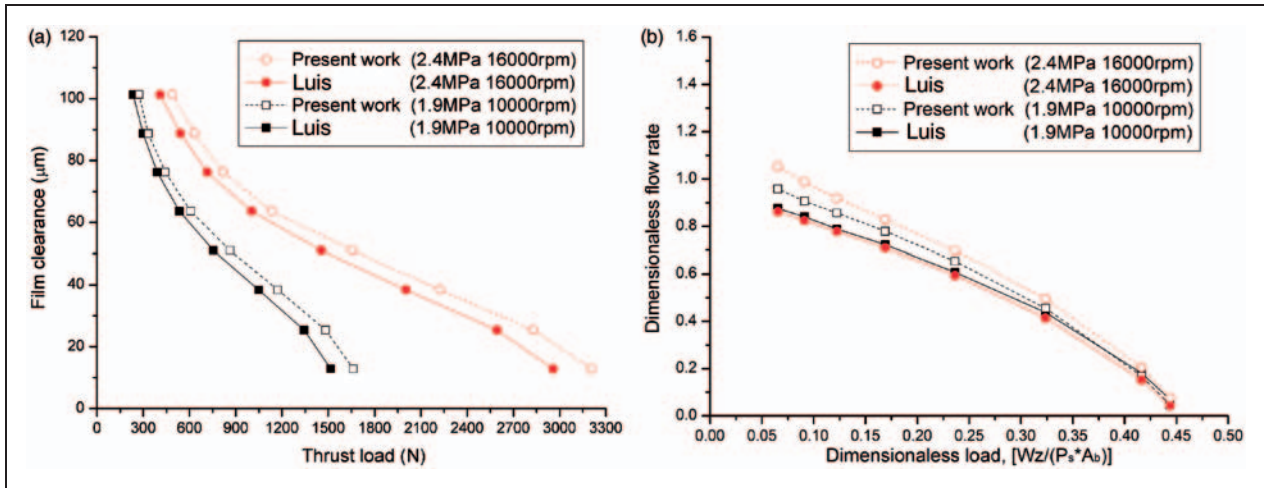


Figure 7. Comparison with the results of Luis.¹⁰

Table 2. Parameters of hydrostatic thrust bearing lubricated by tap water.

Bearing radius (mm)		Nominal film thickness (μm)	Recess depth (mm)	half angle of recess ($^\circ$)
$r_0 = 30r_1 = 33; r_2 = 39; r_3 = 42$		$h_0 = 20$	$h_r = 1$	$\theta = 30$
Orifice diameter (mm)	Supply pressure (MPa)	Eccentricity ratio	Misalignment angle (rad)	
$d_c = 1.0$	$P_s = 1.5, 3$	$t = 0.1 \sim 0.5$	$\alpha = \beta = 1 \sim 3 \times 10^{-4}$	
Rotational speed (r/min)	Viscosity (Pa)	Inlet temperature ($^\circ\text{C}$)	Discharge coefficient	Entrance loss coefficient
$\omega = 2 \sim 4 \times 10^4$	$\mu_0 = 0.001$	$T_0 = 20$	$c_d = 0.8$	$\xi \approx 0.5$

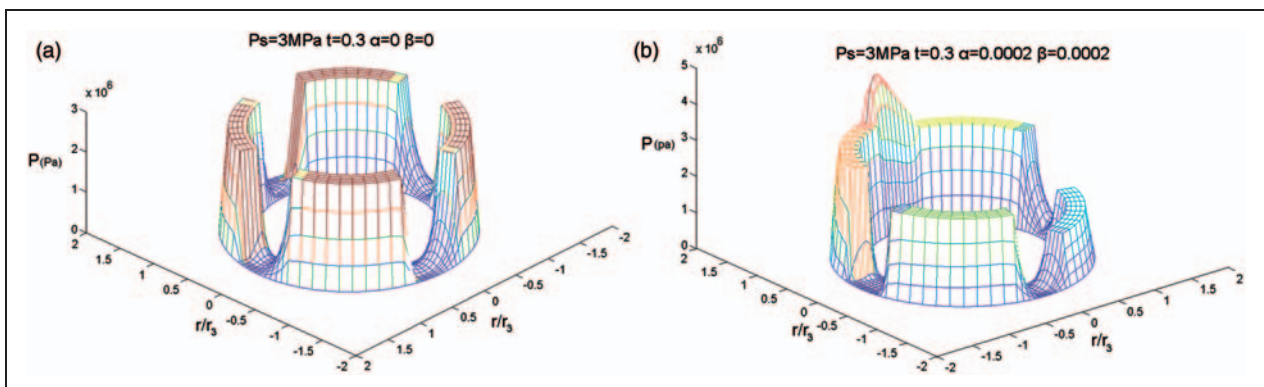


Figure 8. Pressure distribution for water-lubricated hybrid thrust bearing.

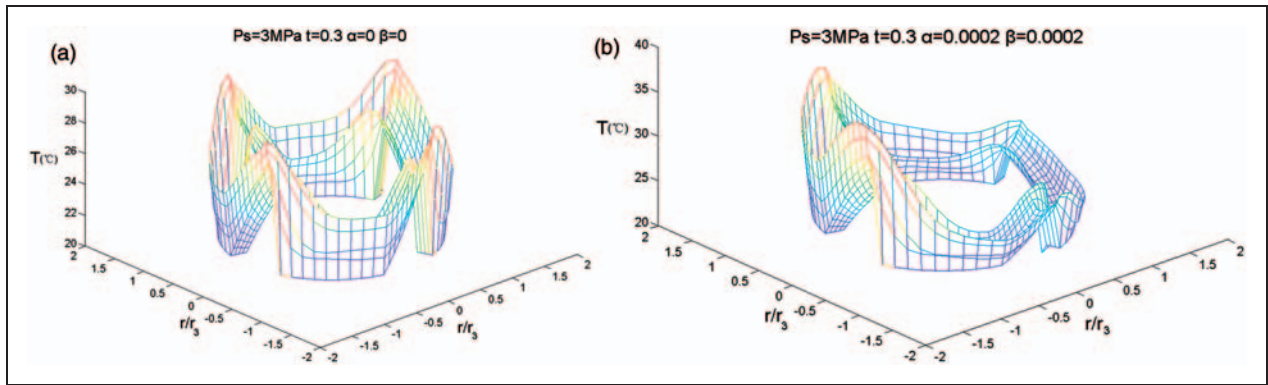


Figure 9. Temperature distribution for water-lubricated hybrid thrust bearing.

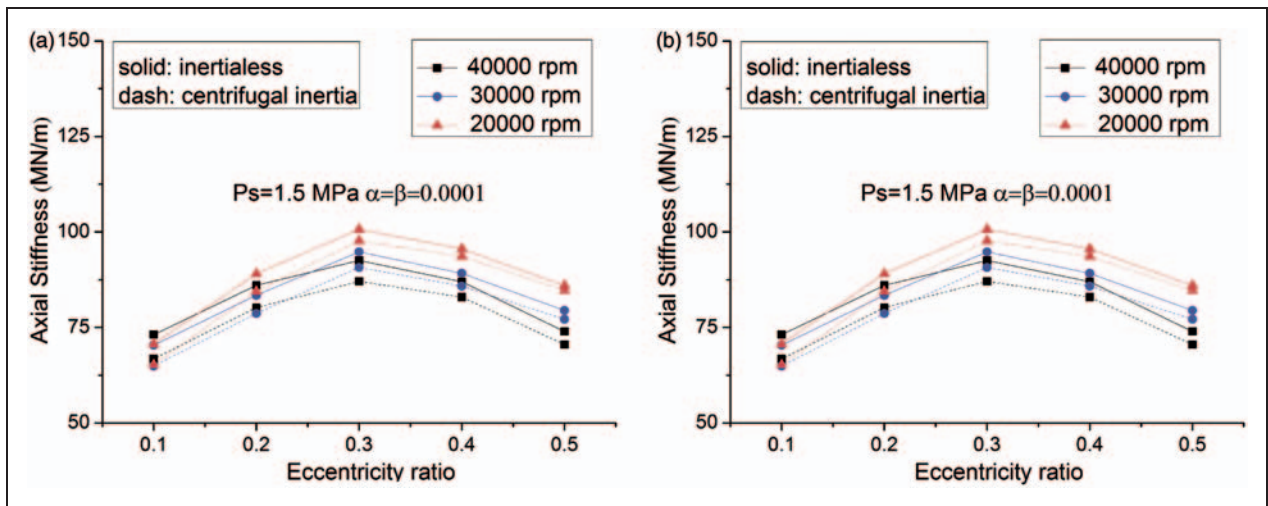


Figure 10. Axial stiffness coefficients versus eccentricity ratio.

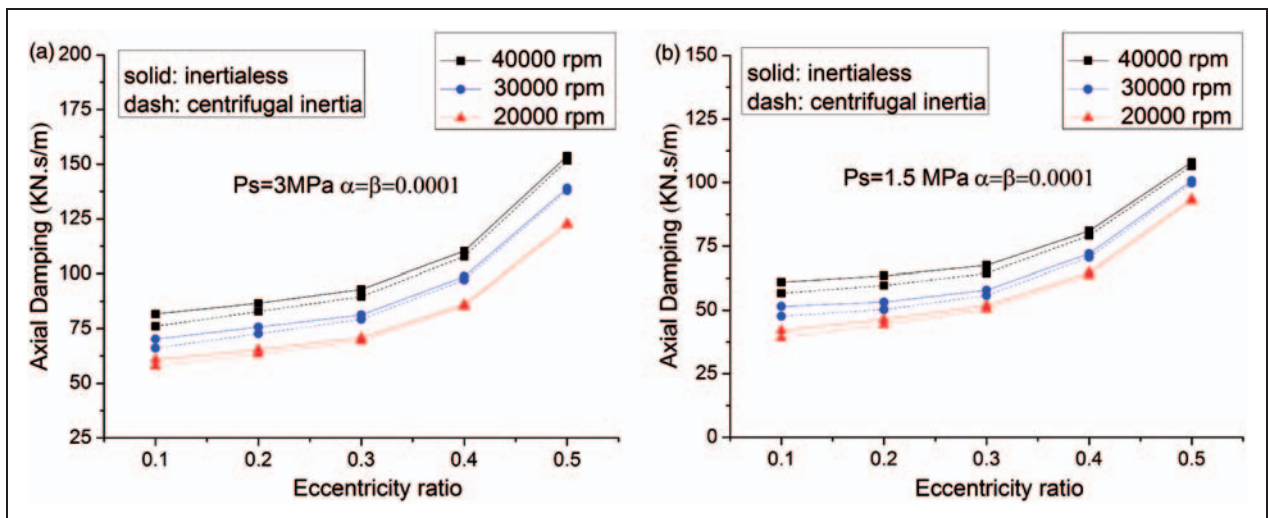


Figure 11. Axial damping coefficients versus eccentricity ratio.

misalignment angle ($\alpha = \beta = <1.5 \times 10^{-4}$ rad). The results also show that the direct angular stiffness coefficient $k_{\alpha\alpha}$ remains relatively constant when the misalignment angle is less than (2.0×10^{-4} rad), while $k_{\alpha\alpha}$

increases rapidly as the misalignment angle exceeds 2.0×10^{-4} rad, the authors think this is caused by the strongly hydrodynamic effect of the bearing. Furthermore, the cross-coupled angular stiffness

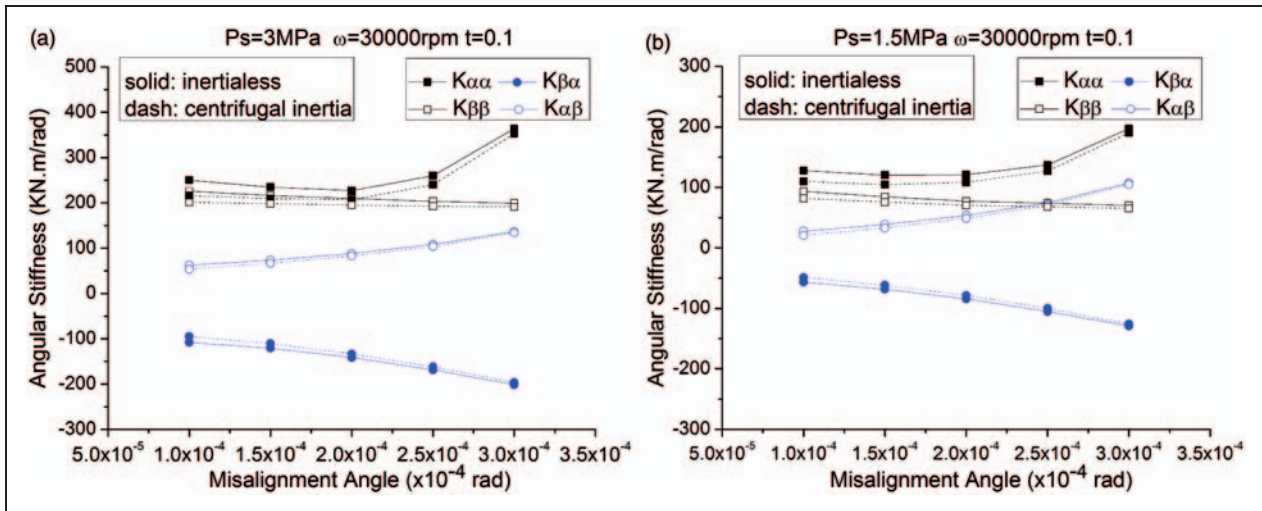


Figure 12. Angular stiffness coefficients versus misalignment angle.

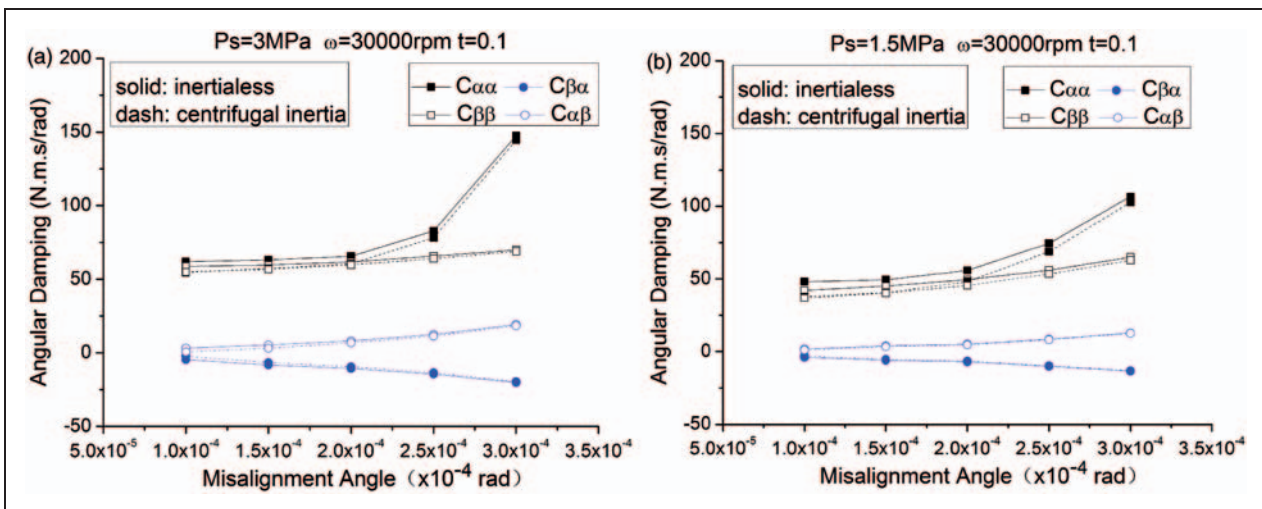


Figure 13. Angular damping coefficients versus misalignment angle.

coefficients increase gradually with the misalignment angles, which are smaller than the direct angular stiffness coefficients.

The angular damping coefficients. The angular damping coefficients as a function of the eccentricity ratio are shown in Figure 13. It is observed that the centrifugal forces also have an influence on the angular damping coefficients, and the direct angular damping coefficients are always greater than the cross-coupled angular damping coefficients. The trend of the variation of $c_{\alpha\alpha}$ is similar as that of $k_{\alpha\alpha}$; in other words, $c_{\alpha\alpha}$ increases rapidly as the misalignment angle exceeds 2.0×10^{-4} rad; a possible explanation is that the water film squeeze effect becomes greater with the decreasing of the local film thickness.

Conclusions

Considering the centrifugal inertia effect, concentrated inertia effect at the recess edge, and the misalignment effect, the thermo-hydrodynamic lubrication model has been established using the reduced Navier–Stokes equation, the energy equation, and the bulk flow theory. The effects of centrifugal forces on the dynamic performances of the high speed water-lubricated thrust bearing with different supply pressures and rotational speeds have been analyzed systematically. The following are the conclusions:

1. The centrifugal inertia effect, concentrated inertia effect at the recess edge, and the misalignment effect significantly affect the pressure and temperature distribution of the high speed hydrostatic

thrust bearing by low viscosity fluid; meanwhile, the centrifugal inertia effect leads to the temperature rise in the radial direction.

2. The centrifugal forces reduce the axial and angular stiffness coefficients and hardly affect the axial and angular damping coefficients of the high speed hydrostatic thrust bearing by low viscosity fluid since the centrifugal forces increase squeeze effect of fluid film to a certain extent.
3. The centrifugal forces have more pronounced effect under higher rotational speed and lower supply pressure. Furthermore, the centrifugal effects decrease with the increasing of the film thickness ratio and the misalignment angle.

Funding

This study was funded by the National Science Foundation (grant numbers 50775036 and 11172065) and the Jiangsu University-Industry Collaboration Project (grant number BY2012199).

Conflict of interest

None declared.

References

1. Abele E, Altintas Y and Brecher C. Machine tool spindle units. *Manuf Technol* 2010; 59(2): 781–802.
2. Liu F, Lin B, Zhang XF, et al. Numerical design method for water-lubricated hybrid sliding bearings. *Int J Precis Eng Manufac* 2008; 9(1): 47–50.
3. Dowson D. Inertia effect in hydrostatic thrust bearing. *ASME J Basic Eng* 1961; 83: 227–234.
4. Coombs JA and Dowson D. An experimental investigation of the effects of lubricant inertia in a hydrostatic thrust bearing. *Proc Instn Mech Engrs* 1964; 179: 96–108.
5. Oscar Pinkus and Lund JW. Centrifugal effects in thrust bearing and seals under laminar condition. *ASME J Lubr Technol* 1981; 103: 126–136.
6. Dareing DW and Chen CM. The contribution of fluid film inertia to the thermodynamic lubrication of sector-pad thrust bearings. *ASME J Lubr Technol Tran* 1976; 98: 125–132.
7. Khalil MF and Ismail AS. Centrifugal effects in externally pressurized bearings under turbulent flow condition. *Tribol Int* 1989; 22: 265–272.
8. Harada M and Aoki H. Analysis of thrust bearings operating in turbulent condition. *ASME J Tribol* 1988; 110: 555–562.
9. Hashimoto H. The effect of fluid inertia forces on the static characteristics of sector-shaped, high speed thrust bearings in turbulent flow regime. *ASME J Tribol* 1989; 111: 406–412.
10. Luis SA. Bulk-flow analysis of hybrid thrust bearings for process fluid applications. *ASME J Tribol* 2000; 122: 170–180.
11. Safar ZS. Centrifugal effects in misaligned hydrostatic thrust bearings. *ASME J Lubr Technol* 1983; 105: 621–624.
12. Luis SA. Effects of misalignment on turbulent flow hybrid thrust bearings. *ASME J Tribol* 2002; 124: 212–219.
13. Ahmad WY, Ashraf SI and Sadek ZK. The combined effects of the centripetal inertia and the surface roughness on the hydrostatic thrust spherical bearings performance. *Tribol Int* 2007; 40: 522–532.
14. Gautam SS, Quamar S and Ghosh MK. Thermal analysis of externally pressurized step bearing including centrifugal inertia effect for a bubbly lubricant. *Int J Eng Sci Technol* 2010; 11(2): 147–166.
15. Pinkus O and Sternlicht B. *Theory of hydrodynamic lubrication*. New York: University Microfilms Publisher, 1961.
16. Constantinescu VN and Galetuse S. Pressure drop due to inertia forces in step bearings. *ASME J Lubr Technol* 1976; 98: 167–174.
17. Bassani R, Ciulli E and Piccigallo B. Hydrostatic lubrication with cryogenic fluids. *Tribol Int* 2006; 39: 827–832.
18. Frene J, Arghir M and Constantinescu V. Combined thin film and Navier-Stokes analysis in high Reynolds number lubrication. *Tribol Int* 2006; 39: 734–747.
19. Arghir M, Attar SE and Nicolas D. Pressure drop in a hydrostatic pocket. Experimental and theoretical results. *Third Body Concept Interpretation Tribol Phenomena* 1996; 31: 423–432.
20. Luis SA. Thermohydrodynamic analysis of fluid film bearings for cryogenic applications. *J Propul Power* 1995; 11(5): 964–972.
21. Zhou Y, Lusi SA and Dara WC. Thermal effects in cryogenic liquid annular seals-part I: theory and approximate solution. *J Tribol* 1993; 115: 267–276.
22. Dai P, Zhang YB and Xu H. The structure of new journal bearing for high-speed machine spindle and its performance. *Lub Eng* 2009; 34(2): 11–14.
23. Charle S, Bonneau O and Frene J. Determination of the discharge coefficient of a thin-walled orifice used in hydrostatic bearings. *J Tribol* 2005; 127(3): 679–684.
24. Luis SA, Zhou Y and Childs D. Turbulent flow hydrostatic bearings: analysis and experimental results. *Int J Mech Sci* 1995; 37(8): 815–829.
25. Szeri AZ. *Fluid film lubrication: theory and design*. New York: Cambridge University Press, 1998.

Appendix

Notation

A_0	orifice sectional area
A_b	bearing surface area
A_r	recess area
C_d	empirical orifice discharge coefficients
C_v	heat capacity of water
E_{in}, E_{out}	the energy flowing into the recess and leaving the boundary of the recess
h_0	nominal film thickness
h	film thickness
h_z, h_α, h_β	{1, $\sin \theta$, $\cos \theta$ }
M_y, M_x	restoring moments on thrust collar
p_a	ambient pressure
p_r	recess pressure
p_s	water supply pressure

p_z, p_α, p_β	perturbed pressure along the axial and angle direction N_{rec} number of the recesses	V_θ, V_r	bulk flow circumferential and radial velocities
Q_{in}, Q_{out}	the flow through the orifice restrictor and the recess outflow into the film lands	α, β	misalignment angle in XZ - Plane and YZ - Plane
Q_{outc}, Q_{outa}	circumferential and radial mass flow	Δh	axial disturbance of the thrust bearing
r_0	bearing inner radius	ξ	empirical entrance loss coefficients
r_1	recess inside radius	θ, r	circumferential and radial coordinates
r_2	recess outside radius	μ_0	dynamic viscosity
r_3	bearing outer radius	ρ	fluid density
t	eccentricity ratio	$\tau_{\theta z}, \tau_{Rz}$	wall shear stresses
T_R	drag torque	$\tau_{\theta z} _0$	turbulent wall shear stress at shaft surface
T_r	the temperature within recess and downstream edge	ω	rotational speed
T_s	water inlet temperature		
T_{left}	temperature in upstream edge		
T_{right}	temperature in downstream edge		
u_θ, u_r, u_z	circumferential, radial and axial velocities		
		Subscripts	
		B, J	bearing and shaft
		r	bearing recesses
		s	the supply condition